Atmospheric Environment 199 (2019) 368–379

Contents lists available at ScienceDirect

Atmospheric Environment

journal homepage: www.elsevier.com/locate/atmosenv

A high-resolution modeling study of a heat wave-driven ozone exceedance event in New York City and surrounding regions

Kaihui Zhao[a,b], Yunxuan Bao[a], Jianping Huang[a,c,*], Yonghua Wu[b], Fred Moshary[b], Mark Arend[b], Yongwei Wang[a], Xuhui Lee[a,d]

[a] Yale-NUIST Center on Atmospheric Environment, International Joint Laboratory on Climate and Environment Change (ILCEC)/ Collaborative Innovation Center on Forecast and Evaluation of Meteorological Disasters (CIC-FEMD), Nanjing University of Information Science & Technology, Nanjing, China
[b] Optical Remote Sensing Laboratory, The City College of New York, New York, NY 10031, USA
[c] I. M. System Group, NOAA/NCEP/Environmental Modeling Center, College Park, MD, 20740, USA
[d] School of Forestry and Environmental Studies, Yale University, New Haven, USA

ARTICLE INFO

Keywords:
Heat wave
New York
Ozone episode
Process analysis
WRF/Chem

ABSTRACT

Heat-wave is one of key meteorological conditions causing the National Ambient Air Quality Standard (NAAQS) exceedance event in urban environment. In this study, the Weather Research and Forecasting model coupled with Chemistry (WRF/Chem) was used to investigate an unusual heat-wave driven ozone (O_3) exceedance event occurring on May 17–19, 2017 in New York City (NYC) and surrounding areas. The WRF/Chem simulations were conducted over the three nested domains with the finest grid spacing of 1.3 km. The simulations were evaluated with various observational data including in situ measurements of air quality and meteorological variables as well as the Lidar-measured vertical profiles. Overall, the WRF/Chem successfully captured the diurnal variations of air quality (e.g., O_3 and nitrogen oxides (NO_x)) and meteorological fields during the event. However, the O_3 was under-predicted during the daytime peak hours but over-predicted during the nighttime. The under-predictions of O_3 were highly associated with over-estimation of the planetary-boundary-layer (PBL) heights and uncertainties of emissions (e.g., NOx, and volatile organic compounds, VOCs), whereas the over-predictions were likely attributed to underestimation of the PBL heights and strong vertical mixing. Several findings are obtained from this study. First, the PBL growth plays a critical role in the development of O_3 episode. The maximum PBLH and the largest PBL growth rates on a high O_3 day are higher than those on a low O_3 day. A strong low-level jet (LLJ) in the lower atmospheric boundary layer with increasing boundary-layer height was observed during the event. Second, the isoprene emissions calculated by the biogenic emission model are underestimated significantly in the WRF/Chem model, which leads to the underprediction of daily O_3 peak values. Third, the process analysis indicates that the local chemical productions are the dominant contributor with the contributions of 63–68% during the ozone-exceedance event.

1. Introduction

O_3 episodes are of great concern due to their detrimental impacts on human health and ecosystem productivity (Council, 1992; Anenberg et al., 2010). O_3 episode is defined as a case when the maximum daily 8h-average (MDA8) O_3 is greater than a threshold value which was 75.0 ppbv and now is strengthened to 70.0 ppbv according to the latest NAAQS (US-EPA, 2017). Heat wave is an extreme weather phenomenon, which poses a major threat to human life (Rooney et al., 1998; Semenza et al., 1996), and produces weather conditions that are conducive to O_3 formation. The negative impact could be aggravated substantially when O_3 episodes and heat waves co-occur (Stedman, 2004; Schnell and Prather, 2017). Anthropogenic and biological emissions are strengthened greatly during heat-wave events (He et al., 2013; Churkina et al., 2017). Favorable meteorological conditions and increased emissions impose an important impact on local contribution to surface O_3 (Mickley et al., 2004; Akimoto, 2003). Meanwhile, regional transport affects ambient levels of surface O_3. O_3 exceedance events are often observed in New York Metropolitan areas as part of Northeast O3 transport region (OTR) during summer months (Zhang and Rao, 1999).

* Corresponding author. Yale-NUIST Center on Atmospheric Environment, International Joint Laboratory on Climate and Environment Change (ILCEC)/ Collaborative Innovation Center on Forecast and Evaluation of Meteorological Disasters (CIC-FEMD), Nanjing University of Information Science & Technology, Nanjing, China.
E-mail address: jianping.huang@noaa.gov (J. Huang).

https://doi.org/10.1016/j.atmosenv.2018.10.059
Received 5 June 2018; Received in revised form 2 October 2018; Accepted 28 October 2018
Available online 31 October 2018
1352-2310/

However, the processes leading to O3 episodes are extremely complicated and the evaluation of their relative contributions remains a large uncertainty (Cohan et al., 2007; Huang et al., 2005). Thus, accurate quantification of relative contribution of individual process is critical to develop a scientific and technological basis of alleviating the impact of O_3 exceedance especially during heat-wave events.

Meteorological conditions are crucial to both local production and regional transport, two key processes driving occurrence of O_3 pollution events. Surface O_3 is a secondary pollutant formed by a series of photochemical reactions involving oxides of nitrogen (NOx = NO + NO_2) and volatile organic compounds (VOCs) in the presence of solar radiation. While average concentrations of air pollutants are controlled primarily by local and regional emissions, air pollution events are mainly driven by meteorological conditions (Logan, 1989; Zhu and Liang, 2013). O_3 episodes are highly associated with weather synoptic patterns that produce favorable meteorological conditions such as high temperature, strong solar radiation, weak winds, and stable atmospheric boundary layer. “Bermuda high” pressure system and Lee-side Trough were identified as the commonly-observed weather synoptic patterns accounting for the O_3 exceedances in New York Metropolitan areas (Pagnotti, 1987). While the synoptic weather patterns produce high temperature favorable for O_3 formation, they serve as a “conveyor belt” and/or mixing mechanism for O_3-rich air mass, demonstrating an important role of regional transport in the elevated levels of ambient O_3. Zhang and Rao (1999) used various surface and upper-air meteorological and air quality observational data to examine the roles of meteorological processes in O_3 formation and accumulation and the relationship between meteorological conditions and O_3 concentrations during a multiday O_3 exceedance event. They noticed that synoptic patterns such as a stagnant or a slow-moving high-pressure system played an important role in the elevated levels of surface O_3 on a regional scale, and local-scale circulation patterns such as land-sea breeze and terrain-induced channeling effect may affect air pollutants transport.

The planetary boundary layer height (PBLH) plays a critical role in the development of ozone episode (e.g., Hu et al., 2014). The role of the PBL varies with the development stages. In the early morning, various anthropogenic emissions of ozone precursors (i.e., NO_x and VOCs) are accumulated near the surface due to the low PBLH. After sunrise, strengthening solar radiation heats surface, turbulence becomes active and inversion layer near surface breaks up. High concentrations of ozone trapped in residual layer aloft are transported down to increase surface ozone quickly. As solar radiation strengthens, the PBL continues to grow until reaching the maximum height. At the mature stage, the higher PBLH facilitates dilution of air pollutants and reduces surface ozone concentrations. On a typical heat-wave day, solar radiation is stronger and the maximum PBLH tends to be higher. The higher PBLH is favorable for dilution and dispersion of air pollutants, but accelerates photochemical reactions of ozone formation. The elevated levels of surface ozone are dependent on the net effect of two opposite roles imposed by the PBLH. On the other hand, the uncertainty of simulating the PBLH on high ozone days is much larger than that on low ozone days (Rao et al., 2003). Thus, accurate quantification of PBL simulations and characterization of the PBL structures on ozone episode days are essential to refine PBL parameterization and eventually improve ozone predictions during ozone episodes.

Biogenic VOC emissions are another factor exerting a great impact on elevated levels of surface O_3. They react with anthropogenic NO_x under favorable meteorological conditions and contribute greatly to photochemical production of surface O_3 on a local scale. During heat-wave events, high temperature substantially increases anthropogenic emissions due to enhanced use of air conditioning and biogenic emissions of VOCs, accelerating photochemical reactions, and eventually deteriorating air quality. Among the hundreds of VOCs emitted from vegetation, isoprene is the most reactive one, contributing greatly to surface O_3 formation. The numerical simulations indicate that the contribution of biogenic VOC emission to O_3 formation is 6–20% in summer months but can be increased to 60% during the heat wave events (Churkina et al., 2017). Although the impacts of temperature on biogenic emissions of VOCs and surface O_3 have been evaluated through sensitive studies (Hass et al., 1997; Schmidt et al., 2001; Simpson et al., 1999), a large uncertainty continues to remain in the estimate of biogenic VOC emissions. For instance, isoprene emissions were underestimated by a factor of two and even up to five on a hot day (Vieno et al., 2010). The uncertainty of isoprene emissions and its impact on enhancement of surface O_3 have not been well quantified in a megacity with dense vegetation cover like NYC during heat-wave events.

Photochemical air quality models as powerful tools have been widely used in the investigation of causal relationship between emissions, meteorology, chemistry, and air pollution events (e.g., Zhang et al., 2006; Doherty et al., 2013; Watson et al., 2016). At a given station or grid point and time period, air pollutant concentrations (e.g., O_3) are highly dependent on emission, transport, dispersion, chemical transformation, and deposition. The simulated changes in chemical species concentrations contributed by individual physical process and chemical reactions at given grid points and time period (e.g., one hour) can be written out for further diagnostic analysis. Such a technique is called process analysis which has been implemented in different numerical air quality models to determine the relative roles of physical processes and chemical reactions in driving air pollutant events (e.g., Jeffries and Tonnesen, 1994; Pu et al., 2017; Khiem et al., 2010). Huang et al. (2005) used an integrated process analysis (IPR) embedded in an operational air quality forecasting model to investigate the relative contributions of individual physical process and chemical reactions to ozone episode development in Hong Kong. The model results indicated that chemical reaction and regional transport contributed about 30% and 70% to the ozone episodes, respectively. The air quality prediction modeling system (AQPMS) simulations with process analysis showed that chemical process and regional transport were the key processes accounting for the ozone exceedances at Mountain Tai and Huang over East China (Wang et al., 2006). Xu et al. (2008) applied a 3-dimensional air-quality model Community Multi-scale Air-Quality (CMAQ) Model of Aerosol Dynamics, Reaction, Ionization, and Dissolution (MADRID) together with process analysis to study a typical O_3 episode in the Beijing. They noticed that O_3 precursors were transported to the urban downwind area by strong transportation processes leading to local chemical production of O_3. Later, the CMAQ together with IPR was used to investigate the formation of ozone in the Yangtze River Delta region, China and the results showed that chemical reactions dominated the ozone change in the urban area and transport process was the main contributor in the surrounding regions (Li et al., 2012). More recently, a regional chemistry-climate model (RegCM-CHEM4) was performed to investigate the mechanism of a heavy ozone pollution event associated with heat wave in Yangtze River Delta region, China and the results showed that chemical reactions played the most important role in ozone formation during heat wave days (Pu et al., 2017). Another regional air quality modeling study using Comprehensive Air Quality Model with Extensions model (CAMx) together with process analysis revealed that the chemical process, vertical diffusion, and horizontal advection had a positive effect on ozone production, and ozone concentrations were decreased by the vertical advection and deposition in Shanghai, a megacity in China (Wu et al., 2017). As a comparison, the studies on process analysis of O_3 formation in United States are relatively less. Jeffries and Tonnesen (1994) implemented this technique into a Lagrangian model to assess the impact of two different photochemical mechanisms on air quality predictions. Jang et al. (1995a, b) incorporated such a method into a high-resolution version of the regional acid deposition model (HR-RADM) to quantify the impact of grid spacing on ozone predictions in the New York areas. However, their process analyses are limited to a single grid cell or a lumped area with a number of grid cells in NYC. To our knowledge, very few numerical

studies are completed with more advanced numerical models and updated emission inventory to quantify the processes governing the ozone episode in NYC and surrounding areas where the heat-wave driven ozone episodes are observed continually in summer time.

NYC is located at the Northeastern United States with an estimated population more than 8 million distributed over a land area of about 784 km^2. NYC features a humid subtropical climate, and the suburbs to the immediate north and west lie in the transitional zone between humid subtropical and humid continental climates. NYC has complex urban terrain and is easily affected by the land-sea breezes (Frizzola and Fisher, 1963; Zhang and Rao, 1999). NYC as a megacity is more vulnerable than other cities or regions to heat-wave events due to enhanced use of electricity and dense population (Bornstein, 1968). The maximum air temperature and surface ozone concentrations can be much higher than that in other cities and regions during heat wave events (Zhang et al., 1998). The densely-covered vegetation in the NYC provides a good chance to evaluate biogenic emissions of isoprene, a key volatile organic species for ozone formation but remaining a large uncertainty. As compared to the general features of meteorological conditions that are conducive to ozone formation as well as the ozone chemistry like ozone formation mechanisms, to our best knowledge, studies of the atmospheric boundary layer structures, biogenic emissions of VOC, and relative contributions of regional transport versus local chemical productions are relatively scarce in NYC.

In this study, a fully coupled "online" WRF/Chem model (Grell et al., 2005) is used to investigate a heat-wave driven ozone exceedance event observed on May 16–19, 2017 in the NYC areas. The WRF/Chem is run for the three nested domains with the finest grid spacing of 1.3 km for better capturing spatial and temporal variations in meteorological fields and surface ozone. Various available observational data including surface relative humidity, temperature, winds, and sounding data are used to evaluate the model performance on simulating meteorological fields and chemical species. The possible reasons causing the model forecast biases are discussed. On the basis of that, a sensitive study is conducted to evaluate the impact of temperature on biogenic isoprene emissions and surface ozone formation during the heat wave event. An IPR is performed to quantify the relative contributions of the major physical processes and chemical reactions to the elevated levels of surface ozone during the event. The main purposes of this paper are to 1) identify the key characteristics of the ABL structures of an ozone episode associated with heat wave, 2) to quantify the uncertainty of the model-calculated emissions of VOC, i.e., isoprene which is highly sensitive to change in surface temperature, and 3) to determine the relative contributions of local photochemical production and regional transport to ozone enhancement during the heat-wave driven episode which can provide scientific evidence to policy-makers for developing emission reduction measures of controlling surface ozone concentrations effectively.

2. Methodology and data

2.1. The modeling system and configurations

The WRF/Chem is a fully coupled regional numerical weather prediction model with chemistry component (Grell et al., 2005). Both meteorological and chemistry components use same horizontal and vertical grids, same physics schemes, and same transport schemes (mass and scalar preserving). The online coupling system enables to avoid the uncertainties resulting from temporal interpolation and grid-mapping associated with offline-coupling. The WRF/Chem has been successfully applied to the regional weather and air quality forecasting, field campaign design, observational interpretations, aerosol-cloud interactions, and climate change research (Fast et al., 2014; Pfister et al., 2017).

Fig. 1 illustrates the model computational domains. The modeling system is run for the three nested domains with grid spacing of 12 km, 4 km, and 1.3 km from the outermost to the innermost domains, respectively. The corresponding grid points are 110 × 85, 100 × 73, and 88 × 61. The outermost domain comprises the eastern United States while the intermediate domain covers New York, New Jersey, Pennsylvania, Massachusetts, and Connecticut. The innermost domain includes the NYC and surrounding regions. There are 46 vertical levels from surface to the 50-hPa level. The height of the lowest vertical layer is about 44 m above the ground level.

National Centers for Environmental Prediction (NCEP) final analysis data at an interval of 6-h with 1° horizontal resolution and 27 vertical levels from surface to the 10-hPa level are used to generate initial and lateral boundary meteorological conditions. Outputs from the Model for Ozone and Related Chemical Tracers Version 4 (MOZART-4/GEOS5) (Emmons et al., 2010) are used to provide chemical initial and lateral conditions to the WRF/Chem simulations. The land use data used in the simulations are based on the 30-arc second United States Geological Survey (USGS) database developed in 2012 (USGS, 2012). Analysis nudging for temperature, wind speed, and geopotential height is performed above the PBL to assure the large-scale circulation be consistent with the reanalysis, and allow model to develop boundary layer dynamics more realistically.

The parameterization schemes used in the WRF/Chem simulations are presented in Table 1. They include microphysics scheme of Lin et al. (1983), Goddard shortwave radiative transfer scheme (Chou and Suarez, 1994), Yonsei University PBL scheme (Hong et al., 2006), Rapid Radiative Transfer Model longwave radiation scheme (Mlawer et al., 1997). Version 2 of the Regional Acid Deposition Model (RADM2) (Stockwell et al., 1990), and Fast-J photolysis scheme (Wild et al., 2000).

Anthropogenic emissions are generated based on the 2011 National Emissions Inventory (NEI) published by the U.S. Environmental Protection Agency (EPA). Hourly weekday emissions for the four major inventory components (point, on-road mobile, non-road mobile, and area) with a 4-km spatial resolution (available at ftp://aftp.fsl.noaa.gov/divisions/taq) are used in this study. The data are currently available for the contiguous 48 states of the United States, southern Canada and northern Mexico (Brioude et al., 2013; Choi and Souri, 2015). Biogenic emissions are calculated online based on Model of Emissions of Gases and Aerosols from Nature (MEGAN) with a 1-km horizontal spatial resolution (Guenther et al., 2006).

2.2. Observational data

Both surface observations and sounding data are used to evaluate the model performance on simulating meteorological variables and air quality species. The surface meteorological data were collected at the weather stations with sampling frequency of 15 min to characterize meteorological conditions within the NYC urban environment (see the locations in Fig. 1). Surface observations consist of near real-time temperature, relative humidity, wind speed and direction. The hourly-averaged raw data are used to validate the model predictions. Air quality data at twelve-site are applied to identify the regional characteristics of the O_3 episode and to validate the model performance. The measurements of O_3 and other species were carried out by the NYSDEC. Sounding data taken at Upton observatory (OKX, 40.87°N, −72.86°E, 20 m above sea level) are used to verify the WRF/Chem-simulated vertical profiles of temperature, relative humidity, and wind speed within the PBL. The data are available twice a day (http://weather.uwyo.edu/upperair/sounding.html).

Ceilometer (Vaisala CL-51) backscatter profiles measured at City College of New York (CCNY, 40.821° N,74.0°W) are another useful data to evaluate the simulated PBLH (Gan et al., 2010). The measurements were taken in a standard measuring mode with 10 m × 770 samples at a data collection interval of 15 seconds. The ceilometer observations show a sharp decrease of aerosols from the top of the PBL to the free atmosphere. In this study, a wavelet covariance transforms method (WCT) is used to determine the PBLH based on the gradient of

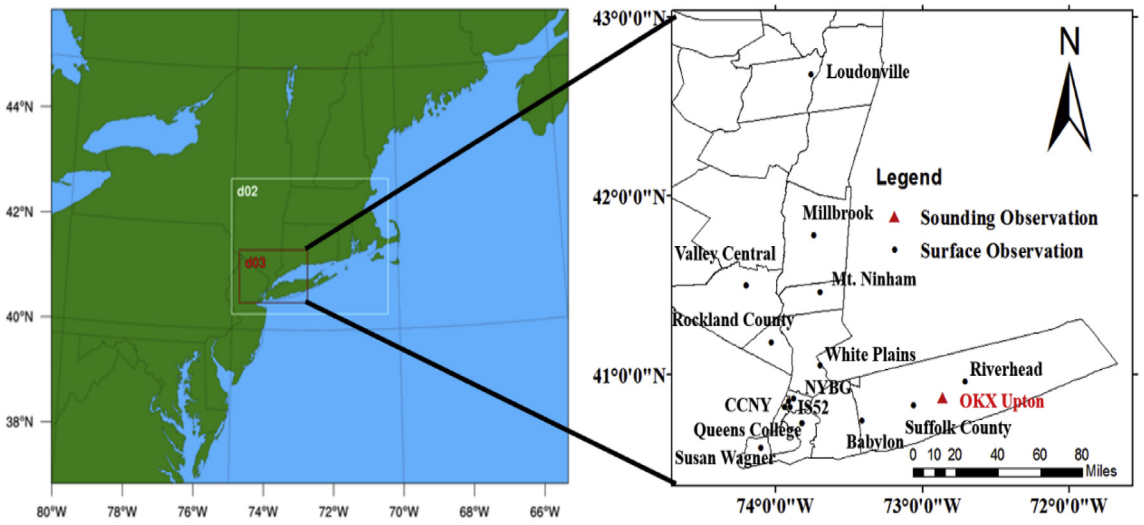

Fig. 1. Nested domains of WRF-Chem model and ozone and sounding observational sites by New York State Department of Environment Conservation(NYSDEC) (black cycle: surface ozone observation; red triangle OKX: sounding observation). (For interpretation of the references to color in this figure legend, the reader is referred to the Web version of this article.)

Table 1
Parameterization schemes used in the WRF/Chem simulations.

Atmospheric process	Parameterization schemes
Microphysics	Lin Microphysics
Shortwave radiation	Goddard
Land-surface option	Noah Land Surface Model
Longwave radiation	Rapid Radiative Transfer Model
Boundary layer	the Yonsei University planetary
Gas phase chemistry	RADM2
Photolysis	Fast-J photolysis

backscatter profiles with a localized impulse Harr function and the maximum covariance between the backscatter profiles and the impulse function (Brooks, 2003; Davis et al., 1997; Gan et al., 2011).

2.3. Process analysis

Process analysis allows for in-depth analysis to understand and quantify the physical processes and chemical reactions involved in the formation of O_3 episodes (Jeffries and Tonnesen, 1994; Jang et al., 1995a,b; Huang et al., 2005). Such a process analysis tool has been implemented in WRF/Chem and applied to quantify the accumulated contributions of individual physical processes (i.e. advection, deposition, vertical mixing) and chemical reactions to the spatial-temporal variations in chemical species (Tao et al., 2015; Gao et al., 2016). Similar to other meteorology/chemistry or air quality models, the time rates of change in chemical species concentrations (C_i) are calculated by using the following mass continuity in WRF/Chem (Jiang et al., 2013):

$$\frac{\partial C_i}{\partial t} = -\left(u\frac{\partial C_i}{\partial x} + v\frac{\partial C_i}{\partial y}\right) - w\frac{\partial C_i}{\partial z} + \frac{\partial}{\partial z}\left(K_e\frac{\partial C_i}{\partial z}\right) + R + D + E, \quad (1)$$

where u, v, and w denote the components of wind speed in x, y, and z directions, respectively; K_e is eddy diffusivity. The six terms on the right-hand side in Eq. (1) represent horizontal advection, vertical advection, vertical diffusion, chemical reactions (R), dry deposition (D), and emissions (E), respectively. A splitting operator method is used to calculate the contribution of each term in Eq. (1). Each term or each process can be written out at each integration time step and each grid point over the innermost domain throughout the simulations.

2.4. Model evaluation metrics

Three threshold statistical indexes are used to validate the model forecast skills. The forecast skill scores include critical success index (*CSI*), false alarm ratio (*FAR*), and probability of detection (*POD*). The *CSI* is a good indicator to reflect the frequency of the episode being predicted. The *FAR* is a parameter indicating the presence of an exceedance event that model predicts when there is no observation. The probability of detection describes the percentage of event which is correctly predicted (Schaefer, 1990). The forecast skill scores are calculated as follows:

$$CSI = \left(\frac{a}{a+b+c}\right) \times 100\%, \quad (2)$$

$$FAR = \left(\frac{b}{a+b}\right) \times 100\%, \quad (3)$$

$$POD = \left(\frac{a}{a+c}\right) \times 100\%, \quad (4)$$

where a represents the number that both forecasts and observations exceed a threshold concentration; b is the number of events that the model predicts but observations do not occur; c denotes the case number that the exceedance events occur but the model is not able to predict; and d indicates the number of occurrences that both model and observation do not show (Schaefer, 1990; Huang et al., 2017). In this study, the model forecast skill scores are calculated for different thresholds of MDA8 for ozone at 60.0 ppbv and 70.0 ppbv.

3. Results and discussion

3.1. Overview of a heat wave-driven O_3 exceedance event

Elevated ambient ozone levels are usually pertinent to the appropriate synoptic patterns (Vukovich, 1995; Zhang and Rao, 1999). The May 18–19, 2017 ozone episode was closely associated with a high pressure situated over the East US with the center located at the Atlantic Ocean, also called the “Bermuda high”, which is one of dominant synoptic patterns driving ozone exceedance events (e.g., Pagnotti, 1987). Such a high-pressure system generated high temperatures, clear skies, and plentiful sunlight that were conducive to ozone photochemical formation. A warm front system centered over the northwest of New York (not shown). The high-pressure system moved

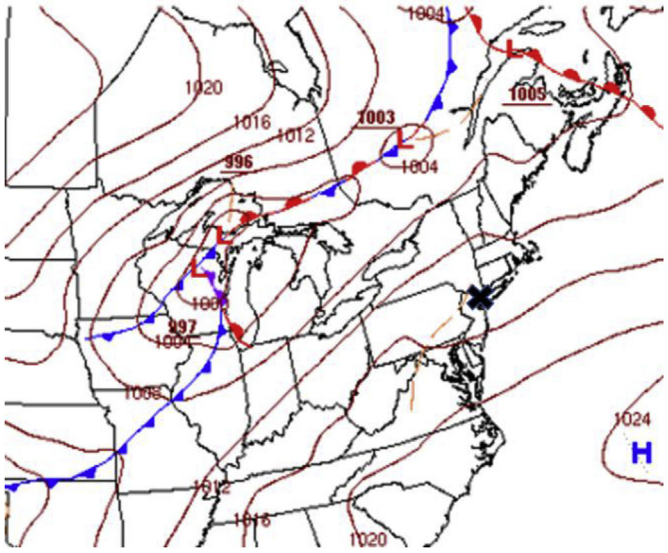

Fig. 2. Surface weather chart at 07 EST on May 18 2017 (black cross: New York City) (from NOAA North American Analysis).

toward northwest and controlled the weather over the NYC. Meanwhile, a quasi-stationary front moved toward northwest of NYC on May 18 (Fig. 2). This synoptic pattern is a typical type for driving occurrence of O_3 episodes in New York. High temperature with clear sky continued to maintain the favorable weather conditions for ozone formation. Influenced by the Appalachian Mountains, prevailing southwest winds associated with the anti-cyclone transported air pollutants from Pennsylvania to NYC. The maximum temperatures in NYC reached 32.0 °C and sustained three consecutive days, which satisfied the heatwave definition criteria (https://www.weather.gov/okx/excessiveheat). The MDA8 for surface ozone reached 80.0 ppbv on 18 May, exceeding the NAAQS for O_3.

3.2. Evaluations of simulated meteorological fields and chemical species

The simulations are conducted from 15 May and lasted for five days. The first 24-h simulations are considered as a spin-up run and the model outputs during the spin-up period aren't included in the statistical evaluations as well as the results analyses. Fig. 3 illustrates a time series comparison of observed 2-m temperature, relative humidity, wind speed, and wind direction at the site Queens College and Yankee (see the locations in Fig. 1) during May 16–19, 2017. During this period, the hourly-average maximum temperature was above 32.5 °C, which indicated a heat wave event in the NYC areas. It is clear that the model was successful in capturing the diurnal variations and trends of key meteorological variable during the event. The temperature showed a steady increasing trend from May 16 to May 19, with the daily maximum 1h-average temperature increasing from 27.7 °C on May 16 to 35.0 °C on May 19 (see Fig. 3a). The relative humidity decreased from 67% to 59% and then followed by a slightly increasing trend during May 17–19. The prevailing southeasterly winds with a wind speed range of 3–5 m s^{-1} transported air with high concentrations of O_3 from southwest and its precursors along the highway I-95 corridor to the NYC areas on May 17–18 (see Fig. 4).

Statistical metrics are calculated to evaluate the WRF-simulated meteorological fields. The statistical metrics include correlation coefficient (*R*), root mean square error (*RMSE*), and mean bias (*MB*). Observational data at sixteen surface sites are used to evaluate the model performance and the verification results for the innermost domain are presented in Table 2. The simulations show a very high correlation coefficients (0.91) for daily 1h-average 2-m temperature but with a slight over-prediction (0.3 °C) for the innermost domain. The correlation coefficient of wind speed is not as high as that of 2-m temperature and relative humidity. Overall, the evaluation results indicate that the model is able to provide reasonable high resolution of surface meteorological inputs to drive the air quality module on simulating spatial and temporal variations of air pollutants.

Fig. 5 shows a comparison of simulated surface ozone with observations at four representative stations during May 16–19 2017. These sites represent the locations with different emission sources and ozone formation regimes in NYC metropolitan areas. In general, the model was able to capture the diurnal variation, the daily peak value, and an increasing trend at different sites, but significantly over-predicted surface ozone concentrations during night time. The statistical evaluation of simulated ozone at twelve surface sites at different isoprene emissions is presented in Table 3. For instance, the ozone was over-predicted by about 30.0 ppbv at night time on May 16 and about 10.0 ppbv on the following day at the Queens College station. Similar performance was observed at other sites such as CCNY and White Plains (Fig. 5c–d). However, a better performance with a correlation coefficient (*R*) of 0.82 and mean bias (*MB*) of −2.21 was found at the Susan Wagner site. Similar over-predictions of ozone during night time were also found in other studies (e.g., Yegorova et al., 2011). The nighttime over-predictions of surface ozone are likely associated with inaccurate meteorological inputs such as under-predicted PBLH and over-predicted eddy diffusivity as well as uncertainties of ozone-precursor emissions (e.g., NOx). However, the under-prediction of ozone peak value during daytime is mainly related to the uncertainties of emissions. For instance, under-estimate of isoprene emission may lead to under-predictions of the daytime ozone peaks.

The day-to-day variability of ozone concentration showed a similar increasing trend to that of temperature from May 16 to 18. With meteorological conditions favorable for O_3 formation, MDA8 ozone went up to 70.0–90.0 ppbv at most of the observational stations including urban and rural sites in the NYC and surrounding regions, leading to violation of the NAAQS for surface ozone. The highest hourly averaged ozone reached to 100.0 ppbv, which was observed at Riverhead site on May 18 (figure not shown). Low ozone concentration (< 10.0 ppbv) was observed at many sites during nighttime on May 17. Ozone concentrations were greatly depressed through the process of NO titration in the immediate vicinity of very large emission of NO. In the meantime, dry deposition with limited ozone rich air transport from aloft was another reason causing very low concentrations of surface ozone during night time (Talbot et al., 2005; Yegorova et al., 2011).

To further investigate the model bias of ozone, simulated NO and NO_2 are compared with the observations at two sites (only data available at Queens College and IS52, see Fig. 1b for their locations) in NYC (Fig. 6). The statistical evaluation of simulated NO and NO_2 is presented in Table 4. Several features are identified from the figure. First, the model was able to mimic the diurnal pattern and day-to-day variation trend for both NO and NO_2 except for a sharp increase of NO at the early morning of May 17. The strong local value was likely associated with the local traffic sources which were not included in the emission inventory. Second, the daily peak NO and NO_2 showed a decreasing trend which was different from that of O_3 as the heat-wave event proceeded. Third, the simulated NO_2 showed opposite performance to simulated-O_3. In other words, while O_3 was over-predicted, NO_2 was under-predicted.

3.3. Characteristics of the atmospheric boundary layers with high ozone

In order to understand how the model-simulated meteorological fields affect ozone simulations, it is important to evaluate the simulated vertical profiles of meteorological fields. The sounding data at the OKX site are used to evaluate the simulated vertical profiles of potential temperature, relative humidity, and wind speed below the 5-km altitude at 7:00 Eastern Standard Time (EST) on May 16-18, 2017. As shown in Fig. 7, the simulated vertical profiles agreed well with the

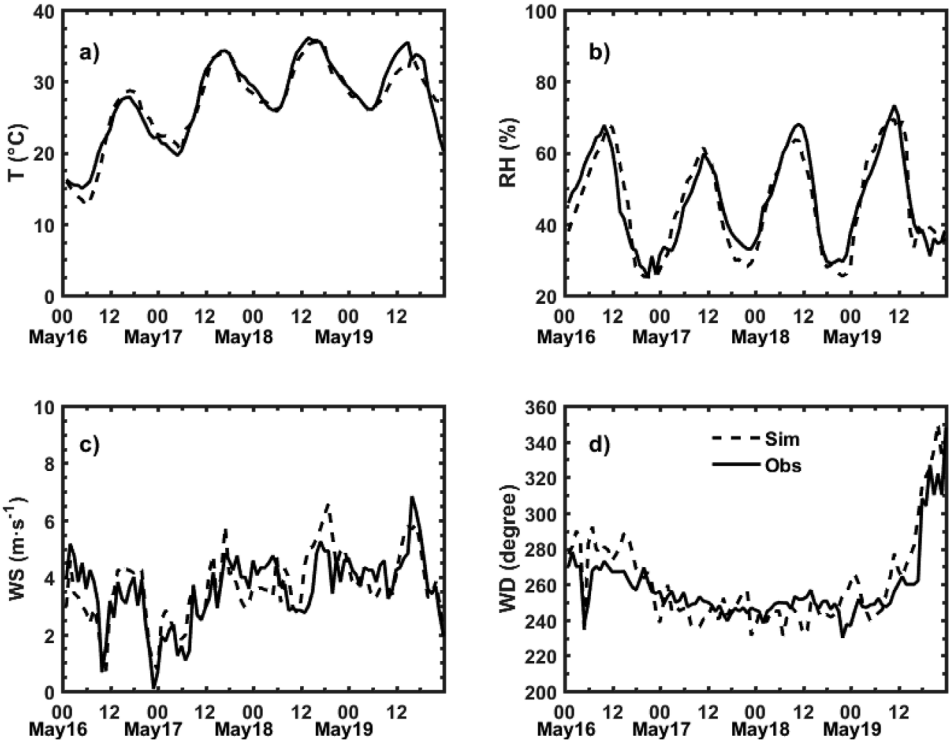

Fig. 3. Time series comparison of simulated (dashed) and observed (solid) a) surface temperature (°C), b) relative humidity (RH, %) at Queens College, c) wind speed (WS, $m{\cdot}s^{-1}$), and d) wind direction (WD, degree) at Yankee.

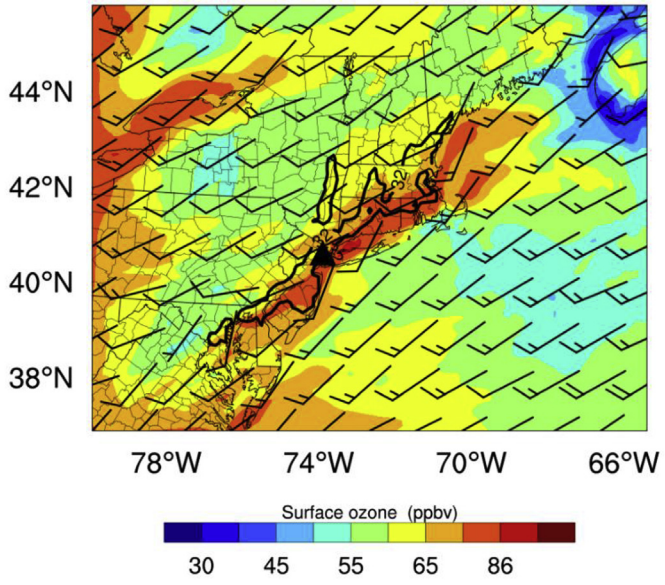

Fig. 4. WRF/Chem predicted surface ozone (shaded colors) and 2-m temperature (black contours for $T_2 >= 32$ °C), wind (black barb) at 14:00 EST on May 18 2017 (black triangle: NYC). (For interpretation of the references to color in this figure legend, the reader is referred to the Web version of this article.)

observations. A strong inversion layer occurred near the surface in the morning (Fig. 7a–b). While the vertical gradients of potential temperatures were increased steadily from 0.007 K m^{-1} on May 16 to 0.023 K m^{-1} on May 18, indicating the increasing stability in the lower troposphere. It is noted that the vertical profiles of relative humidity showed an apparent multiple-layer structure. Meanwhile, a LLJ was observed at the height of about 330 m during the event. The LLJ had an important impact on air pollution transport and diffusion under both aspects, vertical mixing and horizontal transport (Hu et al., 2013).

Table 2
Statistical evaluation of simulated surface meteorological variables and sounding data (R: correlation coefficient; RMSE: root-mean-square error; and MB: mean bias).

	R	RMSE	MB
T	0.91	2.8	0.3
RH	0.80	11.1	0.0
WS	0.59	0.8	0.0
Wind direction	0.64	41.5	−21
T (sounding)	0.99	1.3	−0.8
RH (sounding)	0.90	7.5	0.8
Wind (sounding)	0.75	2.1	0.6

Strong vertical wind shear led to the mechanical production of turbulence through which high concentrations ozone was mixed from the residual layer down to the ground, an important mechanism accounting for the secondary maximum of ozone in the morning. At the same time, it was found that the LLJ may transport air pollutants hundreds-kilometer distance due to high wind speed at the jet core level (Corsmeier et al., 1997). During this event, the maximum wind speed at the LLJ height was reduced from 15.0 m s^{-1} to 12.0 m s^{-1}, indicating an important but slowly weakening role of the LLJ as the event proceeded. The statistical evaluation of simulated vertical meteorological variables is presented in Table 2. Very high correlation coefficients represent the result of the application of objective analysis nudging technique into the simulations. Even though the correlation coefficients of simulated wind speeds are not as high as that of temperature and relative humidity, the evaluations still demonstrate that the model is successful in capturing the vertical profiles.

Fig. 8 illustrates the spatial and temporal variations of attenuated backscatter measured with a ceilometer at CCNY (see Fig. 1b for the location) during May 16–19, 2017. The simulated PBL heights PBLH is included for a direct comparison. As indicated by the high backscatter intensity, aerosols were confined to the lower atmosphere; and the PBLH were determined with the strongest gradient in backscatter

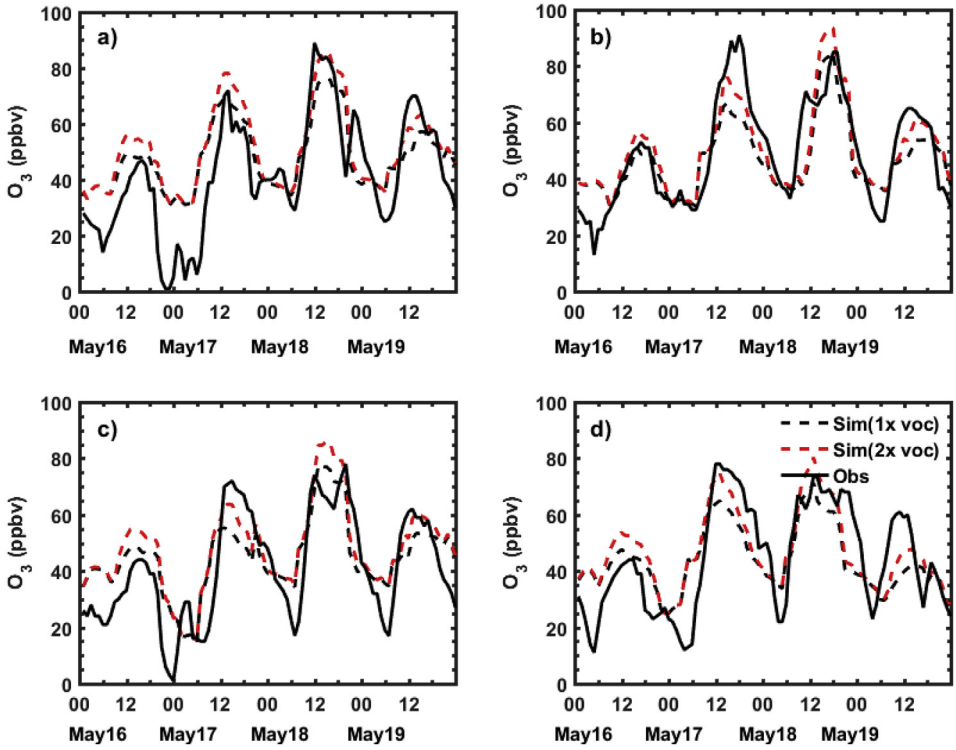

Fig. 5. Time series of simulated (black dashed: 1× isoprene, red dashed: 2× isoprene) and observed (solid) surface O_3 at a) Queens College, b) Susan Wagner, c) CCNY, and d) White Plains. (For interpretation of the references to color in this figure legend, the reader is referred to the Web version of this article.)

Table 3
Evaluation of simulated ozone at different isoprene emissions (R: correlation coefficient, RMSE: root-mean-square error, and MB: mean bias defines, $p < 0.0001$).

	R	RMSE	MB
O_3(1× isoprene)	0.74	9.3	0.3
O_3(2× isoprene)	0.76	12.7	0.4

profile. The simulated maximum PBLH were close to the observations but the development of the simulated PBL started 2–3 h earlier than the observation. A striking feature indicated by the backscatter signal is that the maximum PBLH showed a steady increase during this heat-wave driven ozone episode rather than decreasing trend, which is often observed during a typical air pollution event associated with high concentrations of particulate matters (Petäjä et al., 2016; Zou et al., 2017). This is because that the surface heat flux, a main driver of the PBL development and O_3 formation was increased during the heat-wave event. As indicated by the strong backscatter signal, very little cloud occurred above 3-km during the daytime on May 17–18. The photochemical reactions of ozone became more intensive during May 17–18. However, a low-level cloud was detected by the ceilometer at 2 km from noon to afternoon on May 19; such low-level clouds significantly weakened the shortwave radiation reaching the surface. This explains why the ozone concentrations were decreased on May 19 although the temperature was still very high. Overall, the WRF/Chem model captured the diurnal variation of PBLH in comparison to the observations, as indicated by the high correlation coefficient ($R = 0.78$). But the under-predictions of the PBLH during the nighttime likely resulted from the uncertainty of the PBL scheme.

The impact of the PBL evolution on surface O_3 concentrations is illustrated further in the time-height cross-section plot of O_3 (Fig. 9). It is clear that the PBLH tends to be higher on a heavy O_3-polluted day. For instance, the maximum PBLH on May 18 was 600m higher than that on May 17 (i.e., 2600m versus 2000m). A pool of O_3 with concentration higher than 74 ppbv appeared in the residual layer aloft i.e., above the nocturnal boundary layer, which was transported from the upwind region, i.e., mid-Atlantic region. Such an ozone pool contributed to a rapid increase in surface O_3 concentrations through fumigation and vertical mixing in the morning when the PBL started to grow. The largest hourly growth rate of PBLH was observed at 1000 EST on May 18 with a rate of about 1120 m per hour, which was much higher than that on May 16–17. The largest increase rate of surface O_3 was 10.5 ppbv·h^{-1} which was observed on May 18 at 1100 EST. This indicates a critical role of the PBL growth in the enhancement of surface O_3 during heat-wave driven air pollution event.

3.4. Impact of isoprene emissions on surface ozone predictions

Isoprene emissions are the key biogenic VOC accounting for the enhancement of surface ozone. Fig. 10 shows a time series of simulated biogenic isoprene emissions calculated by MEGAN at Queens College during the event. The isoprene emissions showed a prominent diurnal variation pattern with a steady increasing trend during the event. This is because that the isoprene emissions were mainly driven by solar radiation reaching surface. The strengthening isoprene emissions played a critical role in the enhancement of ozone production, leading the occurrence of ozone exceedance event. The under-predictions of peak ozone were improved when biogenic VOC emissions were increased by 100% (Fig. 5).

Fig. 11 further depicts a scatterplot comparison between simulations and observations for both 8-h average and MDA8 O_3 at the twelve surface observational sites. The 8-hr average ozone was over-predicted when the values were lower than 48.0 ppbv and under-predicted when the values were higher than that value. On the other hand, the MDA8 ozone was always under-predicted. The calculated forecast skill scores demonstrated that the model performed much better at low to moderate ozone concentrations than at high concentrations. For example, the *FAR* at the threshold of 60.0 ppbv was lower than that at the threshold of 70.0 ppbv (5.9% versus 33%), but the corresponding *POD* was higher

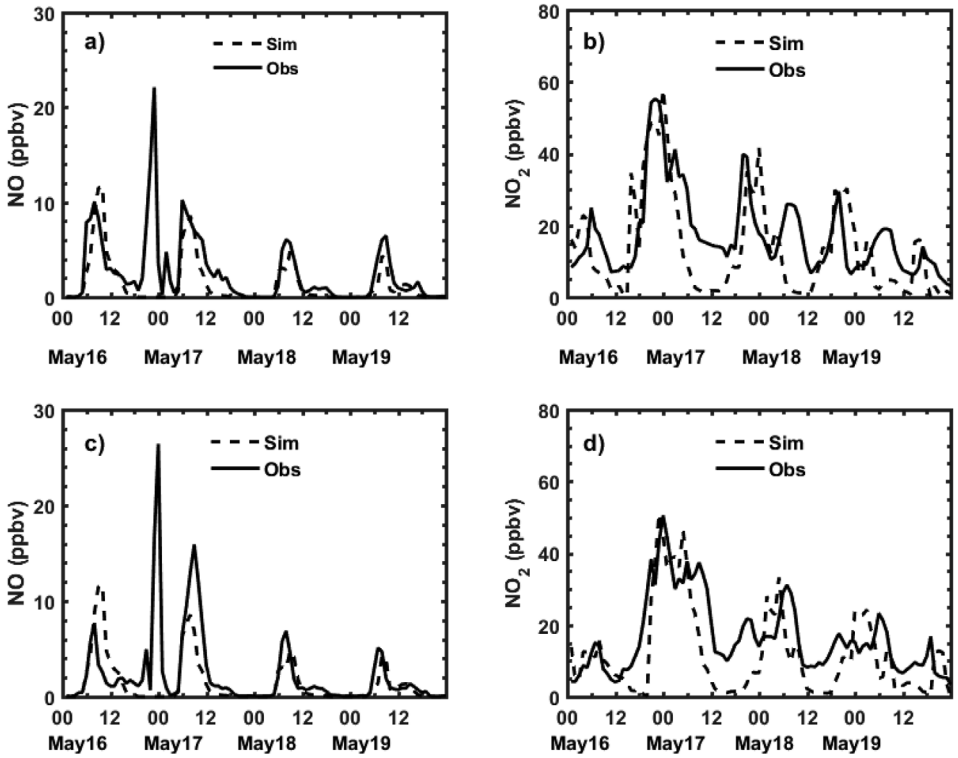

Fig. 6. Time series of simulated (dashed) and observed (solid) surface NO and NO_2 (Unit: ppbv) (a) NO and (b) NO_2 at Queens College, (c) NO and (d) NO_2 at the IS52 site.

Table 4
Statistical evaluation of simulated NO and NO_2 during the event.

	R	RMSE	MB
NO	0.48	3.55	−1.0
NO_2	0.68	15.1	−2.5

(i.e., 67% at the threshold of 60.0 ppbv versus 18% at the thresholds of 70.0 ppbv). Meanwhile, the *CSI* at the threshold of 60.0 ppbv was higher than that at the threshold of 70.0 ppbv (64% versus 17%). The under-prediction of MDA8 was alleviated remarkably and the *POD* of MDA8 was increased to 78% at the thresholds of 60.0 ppbv when the isoprene emissions were increased by one time (see Fig. 5). Meanwhile, the *FAR* was decreased to 4.5% and the *CSI* was increased to 75% at the thresholds of 60.0 ppbv. However, the improvement of forecast skill scores was negligible for the threshold of 70.0 ppbv.

3.5. Local chemical production versus physical contribution

Fig. 12 shows an evolution of simulated ozone vertical profiles averaged over the period of 11:00–16:00 EST for each day during the event. The horizontal region used for process analysis is defined in Fig. 1. This period was selected because the photochemical reactions for ozone formation were the most active. It is seen that ozone in the boundary layer was enhanced from 44.0 ppbv on May 16 to about 74–78.0 ppbv on May 17–18 leading an exceedance of the NAAQS for MAD8 ozone. To better understand processes dominating the exceedance event, the ozone changes associated with different processes were calculated to determine their relative contributions to the total changes of surface ozone. The IPR were conducted for the surface layer to quantify the percentage contribution of the key physical processes and chemical production to the elevated surface ozone levels. The percentage contributions of integrated process to the change in ozone at the surface and the predefined boxes are presented in Table 5. It shows that vertical transport (a sum of vertical advection and vertical diffusion) and chemical production were the two major processes contributing the increase in surface ozone while horizontal advection (or transport) exported ozone from the studied region. Surface ozone was removed partially by dry deposition which was included in other process term during the analysis. Ozone was transported down to the surface due to vertical gradient of ozone in the lower atmospheric boundary layer. The photochemical production showed a positive contribution in NYC urban areas, which was different from what found in other urban areas like Hong Kong where ozone was typically depleted by photochemical production (Huang et al., 2005). To better understand this better, the ratios of VOCs to NOx emissions used in the WRF/Chem simulations were calculated. The ratios varying from 2.9 to 5.6 during the period of 11:00–16:00 LST in the NYC areas, indicate that the ozone precursor emissions with current NEI 2011 version are conducive to ozone formation (Seinfeld, 1991).

As shown in Table 5, the produced ozone through photochemical reactions averaged over the pre-defined region and studying time period was increased from 3 ppbv h^{-1} (25%) on Day 1–6.0 ppbv h^{-1} (68%) on Day 2 and 7.0 ppbv h^{-1} (63%) on Day 3 with increasing air temperature or strengthening solar radiation reaching surface. It is noted that all the processes were interacted to each other. As photochemical production strengthened, the contribution of vertical process was reduced from 9.0 ppbv h^{-1} to 4.1 ppbv h^{-1}. Overall the net change in surface ozone reached 4–7.5 ppbv h^{-1} on May 17–18 when the NAAQS of MDA8 ozone was exceeded. Through the process analysis, it is found that the chemical reactions contributed the significant ozone enhancement most with a percentage of 63–68% during the ozone episode event. The results are consistent with that of Jang et al. (1995a, b), which also shows positive contribution of chemical reactions to the change in ozone concentrations at both 80-km and 20-km resolutions and for a single grid cell and lumped areas in NYC.

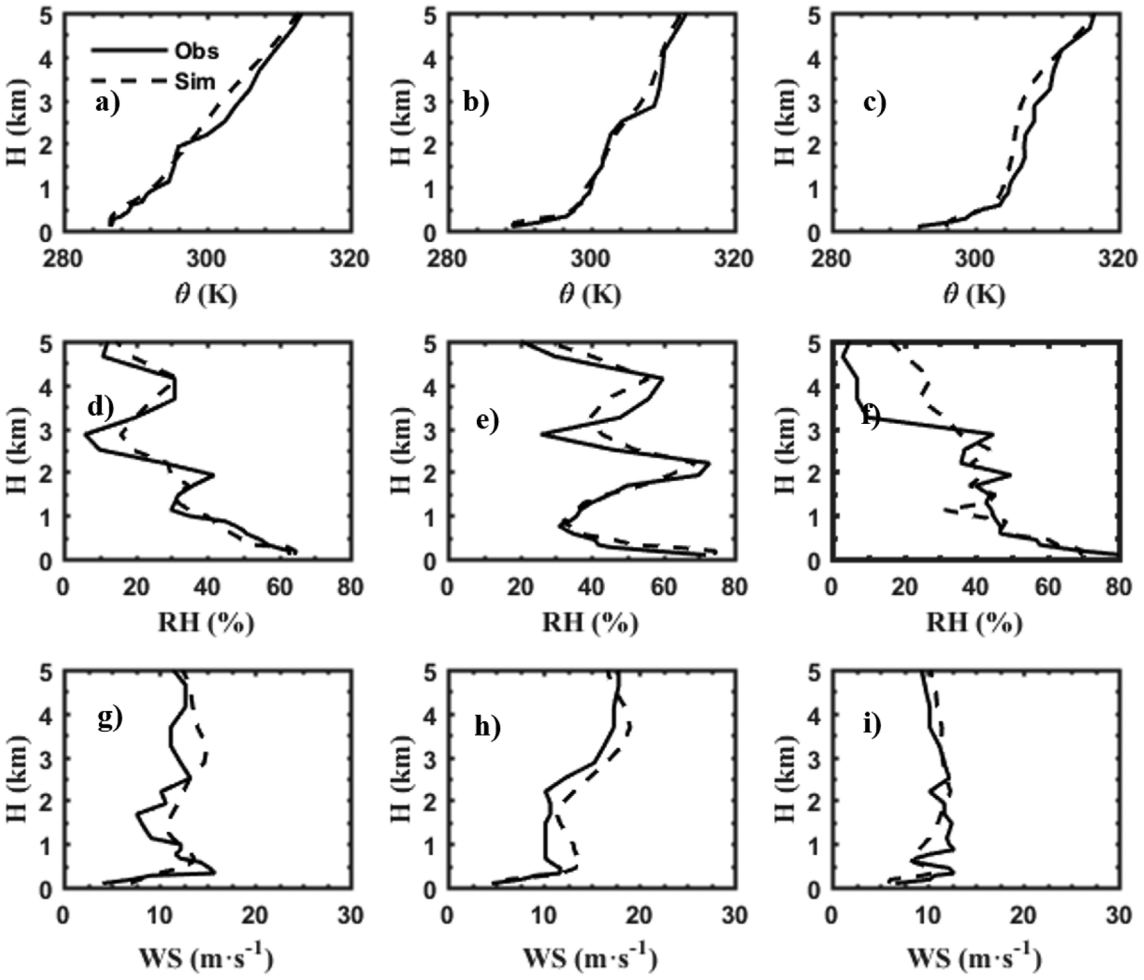

Fig. 7. A comparison of WRF/Chem-simulated vertical profiles with radiosonde observed potential temperature (θ, K), relative humidity (RH, %), and wind speed (WS, $m{\cdot}s^{-1}$) at 07:00 EST, OKX Upton during the event (panels a), d) and g) for May 16; panels b), e), and h) for May 17; and panels c), f) and i) for May 18).

4. Summary and conclusions

A remarkable ozone exceedance event driven by heat wave was observed in New York City and surrounding areas during May 17–18, 2017 with surface temperature higher than 32.0 °C. Such a high temperature together with strong solar radiation and weak wind speed was conducive to ozone formation. A high-resolution model WRF/Chem was used to investigate the relationship between ozone and high temperature and to assess the impact of biogenic emission on elevated surface ozone. The heat wave effect was magnified over the NYC areas

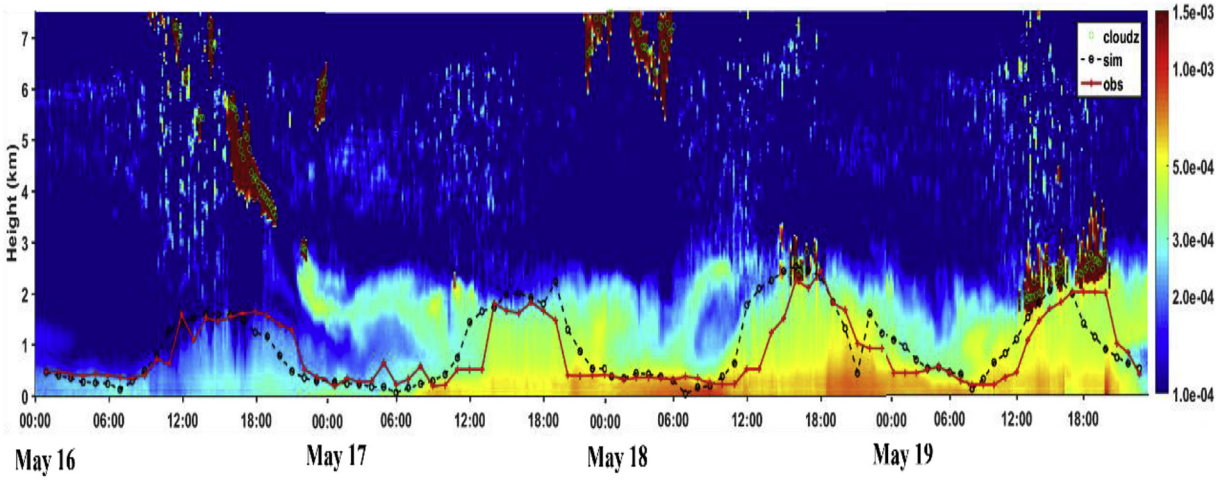

Fig. 8. Spatial and temporal distribution of ceilometer-measured attenuated backscatter ($km^{-1}{\cdot}sr^{-1}$) at CCNY (City College of New York) during May 16–19, 2017 (black line: simulated PBL height; red line: observed PBL height; greed circle: cloud base height). (For interpretation of the references to color in this figure legend, the reader is referred to the Web version of this article.)

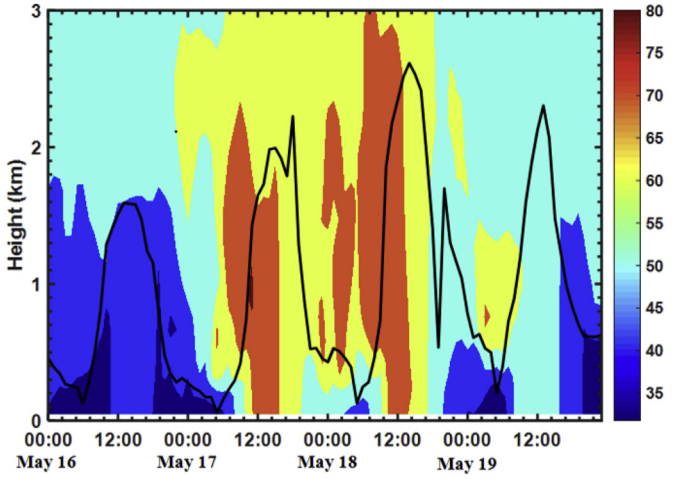

Fig. 9. Time-height cross section plot of simulated O_3 at CCNY during May 16–19, 2017.

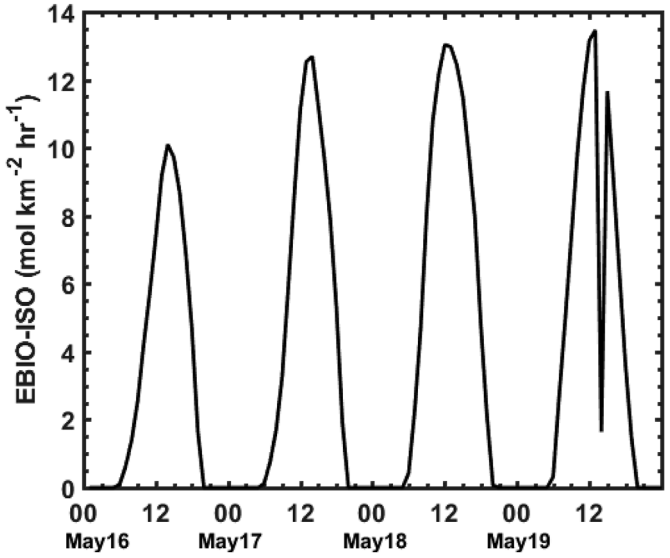

Fig. 10. Time series of simulated biogenic isoprene (mol·km^{-2}·hr^{-1}) at Queens College during May 16–19, 2017.

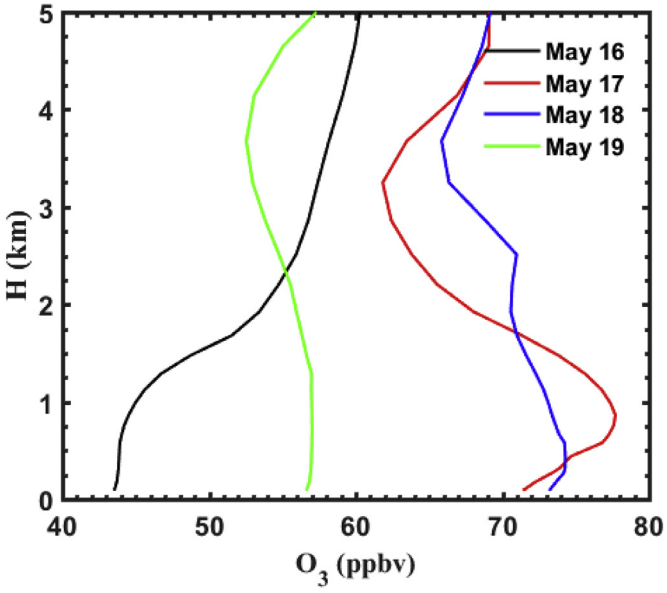

Fig. 12. Vertical profile of simulated ozone (O_3, ppbv) averaged over 11:00–16:00 EST during May 16–19 2017 (black: 16th, red: 17th, blue: 18th, green: 19th). (For interpretation of the references to color in this figure legend, the reader is referred to the Web version of this article.)

by enhancing not only photochemical reaction rates but also ozone precursors emissions. The MD8A ozone was enhanced by 26.8 ppbv while the daily maximum temperature increased 7.8 °C on these two days.

Comparisons between the simulations and the observations demonstrate that the WRF/Chem is successful in reproducing the spatial and temporal variations in meteorological fields, NO, and NO_2 during a heat wave driven ozone exceedance event. Meanwhile the vertical profiles of potential temperature, relative humidity, and wind speed are well represented by the model. High critical success index and probability of detection as well as low false alarm ratio indicate that the high-resolution simulations by WRF/Chem is capable to predict such a heat wave-driven ozone exceedance event. It is noted that the WRF/Chem model overestimated ozone during nighttime and under-predicted ozone peak during daytime. The possible reasons causing the prediction biases were discussed.

Two unique characteristics of the PBL are identified from both modeling and observational analyses for this ozone exceedance event. An increasing rather than decreasing trend of the daily maximum PBLH was observed during the heat-wave driven ozone episode, which is

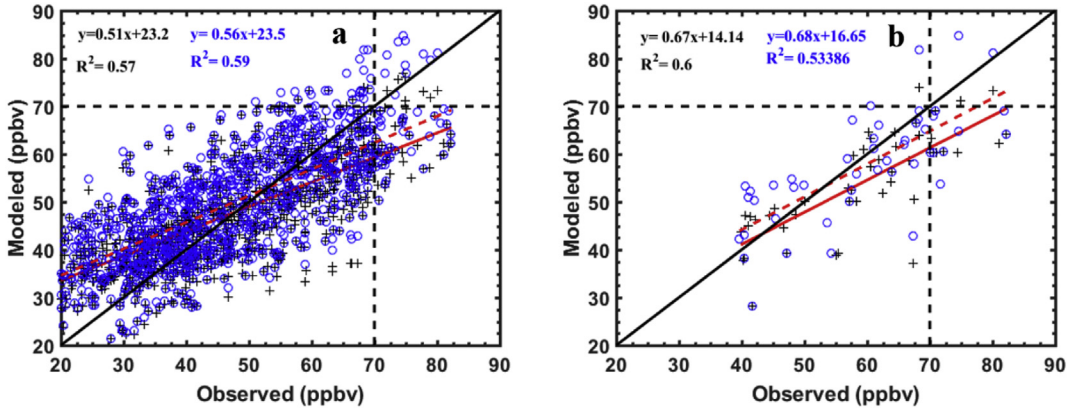

Fig. 11. Scatter plot of the simulated vs. observed a) 8-h average and b) maxima daily 8-hr average O_3 on May 16-19, 2017 (Note: exceedance thresholds: 70.0 ppbv; black plus sign: 1x isoprene; blue circle: 2x isoprene; red solid line: 1x isoprene regression line; red dashed line: 2x isoprene regression line). (For interpretation of the references to color in this figure legend, the reader is referred to the Web version of this article.)

Table 5
Comparisons of the contribution of individual process and the net change at surface.

Date (mon/day)	Horizontal(ppbv·hr^{-1})	Vertical (ppbv·hr^{-1})	Chemical(ppbv·hr^{-1})	Others(ppbv·hr^{-1})	Net(ppbv·hr^{-1})
05/16	−9.5 (92%)	9.0 (75%)	3.0 (25%)	−0.8 (8%)	2.7
05/17	−4.6 (96%)	2.8 (32%)	6.0 (68%)	−0.2 (4%)	4.0
05/18	−2.6 (71%)	4.1 (37%)	7.0 (63%)	−1 (29%)	7.5
05/19	2.9 (38%)	−5.7 (99.99%)	4.6 (62%)	−0.01 (0.01%)	1.8

different from that of a typical particulate-matter air pollution event (Petäjä et al., 2016; Zou et al., 2017). This implies that the accumulation effect of PBL on surface ozone enhancements is not as significant as that on surface aerosol concentrations. Meanwhile, a strong LLJ with a slightly weakening trend was observed at the top of the PBL during night time and early morning.

Sensitive study shows that the biogenic emissions of VOCs such as isoprene may be under-estimated largely by MEGAN. The simulations of peak ozone were improved when the isoprene emissions were increased by 100%. The modeling results also demonstrate that biogenic VOCs can be significantly enhanced during the heat wave event. Therefore, including the impact of biogenic emissions associated with vegetation coverage on air quality is important to develop an effective emission control strategy to reduce high ozone concentrations during an ozone exceedance event.

The process analyses indicate that photochemical reactions were the largest positive contributor to the surface ozone enhancement with percentage contribution of 63–68% on May 17–18 compared to the 25% in the previous day during the ozone episode. The NYC and surrounding regions were highly affected by the chemical process with average contributions of 3 ppbv h^{-1}, 6 ppbv h^{-1}, and 7 ppbv h^{-1} at per hour, respectively. Thus, the results provide a scientific evidence to policy makers on how to control surface ozone concentrations effectively in the NYC and surrounding regions.

This study has an important implication on how to further improve numerical predictions of ozone exceedance event and how to develop emission-reduction measures on controlling surface ozone concentration effectively. The results can be used as a reference for understanding the dominant driving factors (or processes) of ozone episodes in other coastal metropolitan cities like New York.

Acknowledgements

The research was supported jointly by the National Natural Science Foundation of China (Grant 41575009), the National Key Research and Development Program of China (2017YFC0210102), the Xianyang major science and technology projects(2017K01-35), Jiangsu Science and Technology Support Project (BE2014734) and the Priority Academic Program Development of Jiangsu Higher Education Institutions (PAPD), and in part supported by the New York State Energy Resources Development Authority (grant # 100415) and NOAA-CREST under the Cooperative Agreement Grant # NA16SEC4810008. The first author also acknowledges the support Postgraduate Research and Practice Innovation Program of Jiangsu Province (Grant KYLX16_0945). Authors appreciate the surface air quality data from NYSDEC.

Appendix A. Supplementary data

Supplementary data to this article can be found online at https://doi.org/10.1016/j.atmosenv.2018.10.059.

References

Akimoto, H., 2003. Global air quality and pollution. Science 302, 1716–1719.
Anenberg, S.C., Horowitz, L.W., Tong, D.Q., West, J.J., 2010. An estimate of the global burden of anthropogenic ozone and fine particulate matter on premature human mortality using atmospheric modeling. Environ. Health Perspect. 118, 1189.
Bornstein, R.D., 1968. Observations of the urban heat island effect in New York City. J. Appl. Meteorol. 7, 575–582.
Brioude, J., Angevine, W.M., Ahmadov, R., Kim, S.-W., Evan, S., McKeen, S.A., Hsie, E.-Y., Frost, G.J., Neuman, J.A., Pollack, I.B., 2013. Top-down estimate of surface flux in the Los Angeles Basin using a mesoscale inverse modeling technique: assessing anthropogenic emissions of CO, NO x and CO 2 and their impacts. Atmos. Chem. Phys. 13, 3661–3677.
Brooks, I.M., 2003. Finding boundary layer top: application of a wavelet covariance transform to lidar backscatter profiles. J. Atmos. Ocean. Technol. 20, 1092–1105.
Choi, Y., Souri, A.H., 2015. Chemical condition and surface ozone in large cities of Texas during the last decade: observational evidence from OMI, CAMS, and model analysis. Remote Sens. Environ. 168, 90–101.
Chou, M.-D., Suarez, M.J., 1994. An efficient thermal infrared radiation parameterization for use in general circulation models. Citeseer 3 NASA Tech. Memo. 104606, 85pp. [Available from NASA/GoddardSpace Flight Center, Code 913, Greenbelt, MD 20771].
Churkina, G., Kuik, F., Bonn, B., Lauer, A., Grote, R., Tomiak, K., Butler, T.M., 2017. Effect of VOC emissions from vegetation on air quality in Berlin during a heatwave. Environ. Sci. Technol. 51, 6120–6130.
Cohan, D.S., Boylan, J.W., Marmur, A., Khan, M.N., 2007. An integrated framework for multipollutant air quality management and its application in Georgia. Environ. Manag. 40, 545–554.
Corsmeier, U., Kalthoff, N., Kolle, O., Kotzian, M., Fiedler, F., 1997. Ozone concentration jump in the stable nocturnal boundary layer during a LLJ-event. Atmos. Environ. 31, 1977–1989.
Council, N.R., 1992. Rethinking the Ozone Problem in Urban and Regional Air Pollution. National Academies Press.
Davis, K.J., Lenschow, D.H., Oncley, S.P., Kiemle, C., Ehret, G., Giez, A., Mann, J., 1997. Role of entrainment in surface-atmosphere interactions over the boreal forest. J. Geophys. Res. Atmos. 102, 29219–29230.
Doherty, R.M., Wild, O., Shindell, D.T., Zeng, G., MacKenzie, I.A., Collins, W.J., Fiore, A.M., Stevenson, D.S., Dentener, F.J., Schultz, M.G., 2013. Impacts of climate change on surface ozone and intercontinental ozone pollution: a multi-model study. J. Geophys. Res. Atmos. 118, 3744–3763.
Emmons, L.K., Walters, S., Hess, P.G., Lamarque, J.-F., Pfister, G.G., Fillmore, D., Granier, C., Guenther, A., Kinnison, D., Laepple, T., 2010. Description and Evaluation of the Model for Ozone and Related Chemical Tracers. version 4 (MOZART-4).
Fast, J.D., Craven, J., Metcalf, A., Seinfeld, J.H., 2014. Modeling regional aerosol and aerosol precursor variability over California and its sensitivity to emissions and long-range transport during the 2010 CalNex and CARES campaigns. Atmos. Chem. Phys. 14, 10013–10060.
Frizzola, J.A., Fisher, E.L., 1963. A series of sea breeze observations in the New York City area. J. Appl. Meteorol. 2, 722–739.
Gan, C.-M., Wu, Y., Madhavan, B.L., Gross, B., Moshary, F., 2011. Application of active optical sensors to probe the vertical structure of the urban boundary layer and assess anomalies in air quality model PM2. 5 forecasts. Atmos. Environ. 45, 6613–6621.
Gan, C.M., Wu, Y., Gross, B., Moshary, F., 2010. Statistical comparison between hysplit sounding and lidar observation of planetary boundary layer characteristics over New York City. In: Laser Radar Technology and Applications Xv. International Society for Optics and Photonics, pp. 76841K.
Gao, J., Zhu, B., Xiao, H., Kang, H., Hou, X., Shao, P., 2016. A case study of surface ozone source apportionment during a high concentration episode, under frequent shifting wind conditions over the Yangtze River Delta, China. Sci. Total Environ. 544, 853–863.
Grell, G.A., Peckham, S.E., Schmitz, R., McKeen, S.A., Frost, G., Skamarock, W.C., Eder, B., 2005. Fully coupled "online" chemistry within the WRF model. Atmos. Environ. 39, 6957–6975.
Guenther, A., Karl, T., Harley, P., Wiedinmyer, C., Palmer, P.I., Geron, C., 2006. Estimates of global terrestrial isoprene emissions using MEGAN (model of emissions of gases and aerosols from nature). Atmos. Chem. Phys. 6, 3181–3210.
Hass, H., Builtjes, P.J.H., Simpson, D., Sternii, R., 1997. Comparison of model results obtained with several European regional air quality models. Atmos. Environ. 31, 3259–3279.
He, H., Hembeck, L., Hosley, K.M., Canty, T.P., Salawitch, R.J., Dickerson, R.R., 2013. High ozone concentrations on hot days: the role of electric power demand and NOx emissions. Geophys. Res. Lett. 40, 5291–5294.
Hong, S.-Y., Noh, Y., Dudhia, J., 2006. A new vertical diffusion package with an explicit treatment of entrainment processes. Mon. Weather Rev. 134, 2318–2341.
Hu, X.-M., Klein, P., Xue, M., Zhang, F., Doughty, D., Forkel, R., Joseph, E., Fuentes, J.D., 2013. Impact of the vertical mixing induced by low-level jets on boundary layer ozone concentration. Atmos. Environ. 70, 123–130.
Hu, X.-M., et al., 2014. Impact of the loess plateau on the atmospheric boundary layer structure and air quality in the north China plain: a case study. Sci. Total Environ.

https://doi.org/10.1016/j.scitotenv.2014.08.053.
Huang, J., Fung, J.C.H., Lau, A.K.H., Qin, Y., 2005. Numerical simulation and process analysis of typhoon-related ozone episodes in Hong Kong. J. Geophys. Res. Atmos. 110.
Huang, J., McQueen, J., Wilczak, J., Djalalova, I., Stajner, I., Shafran, P., Allured, D., Lee, P., Pan, L., Tong, D., 2017. Improving NOAA NAQFC PM2. 5 predictions with a bias correction approach. Weather Forecast. 32, 407–421.
Jang, J.-C.C., Jeffries, H.E., Byun, D., Pleim, J.E., 1995a. Sensitivity of ozone to model grid resolution—I. Application of high-resolution regional acid deposition model. Atmos. Environ. 29, 3085–3100.
Jang, J.-C.C., Jeffries, H.E., Tonnesen, S., 1995b. Sensitivity of ozone to model grid resolution—II. Detailed process analysis for ozone chemistry. Atmos. Environ. 29, 3101–3114.
Jeffries, H.E., Tonnesen, S., 1994. A comparison of two photochemical reaction mechanisms using mass balance and process analysis. Atmos. Environ. 28, 2991–3003.
Jiang, Z., Liu, Z., Wang, T., Schwartz, C.S., Lin, H., Jiang, F., 2013. Probing into the impact of 3DVAR assimilation of surface PM10 observations over China using process analysis. J. Geophys. Res. Atmos. 118, 6738–6749.
Khiem, M., Ooka, R., Hayami, H., Yoshikado, H., Huang, H., Kawamoto, Y., 2010. Process analysis of ozone formation under different weather conditions over the Kanto region of Japan using the MM5/CMAQ modelling system. Atmos. Environ. 44, 4463–4473.
Li, L., Chen, C.H., Huang, C., Huang, H.Y., Zhang, G.F., Wang, Y.J., Wang, H.L., Lou, S.R., Qiao, L.P., Zhou, M., 2012. Process analysis of regional ozone formation over the Yangtze River Delta, China using the Community Multi-scale Air Quality modeling system. Atmos. Chem. Phys. 12, 10971–10987.
Lin, Y.-L., Farley, R.D., Orville, H.D., 1983. Bulk parameterization of the snow field in a cloud model. J. Clim. Appl. Meteorol. 22, 1065–1092.
Logan, J.A., 1989. Ozone in rural areas of the United States. J. Geophys. Res. Atmos. 94, 8511–8532.
Mickley, L.J., Jacob, D.J., Field, B.D., Rind, D., 2004. Effects of future climate change on regional air pollution episodes in the United States. Geophys. Res. Lett. 31.
Mlawer, E.J., Taubman, S.J., Brown, P.D., Iacono, M.J., Clough, S.A., 1997. Radiative transfer for inhomogeneous atmospheres: RRTM, a validated correlated-k model for the longwave. J. Geophys. Res. Atmos. 102, 16663–16682.
Pagnotti, V., 1987. A meso-meteorological feature associated with high ozone concentrations in the northeastern United States. JAPCA 37, 720–722.
Petäjä, T., Järvi, L., Kerminen, V.-M., Ding, A.J., Sun, J.N., Nie, W., Kujansuu, J., Virkkula, A., Yang, X., Fu, C.B., 2016. Enhanced air pollution via aerosol-boundary layer feedback in China. Sci. Rep. 6, 18998.
Pfister, G.G., Reddy, P.J., Barth, M.C., Flocke, F.F., Fried, A., Herndon, S.C., Sive, B.C., Sullivan, J.T., Thompson, A.M., Yacovitch, T.I., 2017. Using observations and source-specific model Tracers to characterize pollutant transport during FRAPPÉ and DISCOVER-AQ. J. Geophys. Res. Atmos. 122.
Pu, X., Wang, T.J., Huang, X., Melas, D., Zanis, P., Papanastasiou, D.K., Poupkou, A., 2017. Enhanced surface ozone during the heat wave of 2013 in Yangtze River Delta region, China. Sci. Total Environ. 603, 807–816.
Rao, S.T., Jia-Yeong, K.U., Berman, S., Zhang, K., Mao, H., 2003. Summertime characteristics of the atmospheric boundary layer and relationships to ozone levels over the eastern United States. In: Air Quality. Springer, pp. 21–55.
Rooney, C.M., Smith, C.A., Ng, C.Y.C., Loftin, S.K., Sixbey, J.W., Gan, Y., Srivastava, D.-K., Bowman, L.C., Krance, R.A., Brenner, M.K., 1998. Infusion of cytotoxic T cells for the prevention and treatment of Epstein-Barr virus–induced lymphoma in allogeneic transplant recipients. Blood 92, 1549–1555.
Schaefer, J.T., 1990. The critical success index as an indicator of warning skill. Weather Forecast. 5, 570–575.
Schmidt, H., Derognat, C., Vautard, R., Beekmann, M., 2001. A comparison of simulated and observed ozone mixing ratios for the summer of 1998 in Western Europe. Atmos. Environ. 35, 6277–6297.
Schnell, J.L., Prather, M.J., 2017. Co-occurrence of extremes in surface ozone, particulate matter, and temperature over eastern North America. Proc. Natl. Acad. Sci. 114, 2854–2859. https://doi.org/10.1073/pnas.1614453114.
Semenza, G.L., Jiang, B.-H., Leung, S.W., Passantino, R., Concordet, J.-P., Maire, P., Giallongo, A., 1996. Hypoxia response elements in the aldolase A, enolase 1, and lactate dehydrogenase A gene promoters contain essential binding sites for hypoxia-inducible factor 1. J. Biol. Chem. 271, 32529–32537.
Seinfeld, J.H., 1991. Rethinking the Ozone Problem in Urban and Regional Air Pollution.
Simpson, D., Winiwarter, W., Börjesson, G., Cinderby, S., Ferreiro, A., Guenther, A., Hewitt, C.N., Janson, R., Khalil, M.A.K., Owen, S., 1999. Inventorying emissions from nature in Europe. J. Geophys. Res. Atmos. 104, 8113–8152.
Stedman, J.R., 2004. The predicted number of air pollution related deaths in the UK during the August 2003 heatwave. Atmos. Environ. 38, 1087–1090.
Stockwell, W.R., Middleton, P., Chang, J.S., Tang, X., 1990. The second generation regional acid deposition model chemical mechanism for regional air quality modeling. J. Geophys. Res. Atmos. 95, 16343–16367.
Talbot, R., Mao, H., Sive, B., 2005. Diurnal characteristics of surface level O3 and other important trace gases in New England. J. Geophys. Res. Atmos. 110.
Tao, W., Liu, J., Ban-Weiss, G.A., Hauglustaine, D.A., Zhang, L., Zhang, Q., Cheng, Y., Yu, Y., Tao, S., 2015. Effects of urban land expansion on the regional meteorology and air quality of eastern China. Atmos. Chem. Phys. 15, 8597.
USEPA, 2017, https://www.epa.gov/criteria-air-pollutants/naaqs-table.
USGS, 2012. http://www2.mmm.ucar.edu/wrf/users/download/get_sources.html, Accessed in January 2012.
Vieno, M., Dore, A.J., Stevenson, D.S., Doherty, R., Heal, M.R., Reis, S., Hallsworth, S., Tarrason, L., Wind, P., Fowler, D., Simpson, D., Sutton, M.A., 2010. Modelling surface ozone during the 2003 heat-wave in the UK. Atmos. Chem. Phys. 10, 7963–7978. https://doi.org/10.5194/acp-10-7963-2010.
Vukovich, F.M., 1995. Regional-scale boundary layer ozone variations in the eastern United States and their association with meteorological variations. Atmos. Environ. 29, 2259–2273.
Wang, Z., Li, J., Wang, X., Pochanart, P., Akimoto, H., 2006. Modeling of regional high ozone episode observed at two mountain sites (Mt. Tai and Huang) in East China. J. Atmos. Chem. 55, 253–272.
Watson, L., Lacressonnière, G., Gauss, M., Engardt, M., Andersson, C., Josse, B., Marécal, V., Nyiri, A., Sobolowski, S., Siour, G., 2016. Impact of emissions and + 2° C climate change upon future ozone and nitrogen dioxide over Europe. Atmos. Environ. 142, 271–285.
Wild, O., Zhu, X., Prather, M.J., 2000. Fast-J: accurate simulation of in-and below-cloud photolysis in tropospheric chemical models. J. Atmos. Chem. 37, 245–282.
Wu, J., Wang, Q., Chen, H., Zhang, Y., Wild, O., 2017. On the origin of surface ozone episode in Shanghai over Yangtze River Delta during a prolonged heat wave. Aerosol Air Qual. Res. 17, 2804–2815.
Xu, J., Zhang, Y., Fu, J.S., Zheng, S., Wang, W., 2008. Process analysis of typical summertime ozone episodes over the Beijing area. Sci. Total Environ. 399, 147–157. https://doi.org/10.1016/j.scitotenv.2008.02.013.
Yegorova, E.A., Allen, D.J., Loughner, C.P., Pickering, K.E., Dickerson, R.R., 2011. Characterization of an eastern US severe air pollution episode using WRF/Chem. J. Geophys. Res. Atmos. 116.
Zhang, J., Rao, S.T., 1999. The role of vertical mixing in the temporal evolution of ground-level ozone concentrations. J. Appl. Meteorol. 38, 1674–1691.
Zhang, J., Rao, S.T., Daggupaty, S.M., 1998. Meteorological processes and ozone exceedances in the northeastern United States during the 12–16 July 1995 episode. J. Appl. Meteorol. 37, 776–789.
Zhang, Y., Liu, P., Queen, A., Misenis, C., Pun, B., Seigneur, C., Wu, S.-Y., 2006. A comprehensive performance evaluation of MM5-CMAQ for the Summer 1999 Southern Oxidants Study episode—Part II: gas and aerosol predictions. Atmos. Environ. 40, 4839–4855.
Zhu, J., Liang, X.-Z., 2013. Impacts of the Bermuda high on regional climate and ozone over the United States. J. Clim. 26, 1018–1032.
Zou, J., Sun, J., Ding, A., Wang, M., Guo, W., Fu, C., 2017. Observation-based estimation of aerosol-induced reduction of planetary boundary layer height. Adv. Atmos. Sci. 34, 1057–1068.